minerals

MDPI

Article

Whitlockite-Type Structure as a Matrix for Optical Materials: Synthesis and Characterization of Novel TM-SM Co-Doped Phosphate $Ca_9Gd(PO_4)_7$, a Single-Phase White Light Phosphors

Ivan V. Nikiforov [1], Dina V. Deyneko [1,2], Dmitry A. Spassky [3,4], Bogdan I. Lazoryak [1] and Sergey M. Aksenov [2,5,*]

[1] Department of Chemistry, Lomonosov Moscow State University, 119991 Moscow, Russia; ivan.nikiforov@chemistry.msu.ru (I.V.N.); deynekomsu@gmail.com (D.V.D.); bilazoryaka@gmail.com (B.I.L.)
[2] Laboratory of Arctic Mineralogy and Material Sciences, Kola Science Centre, Russian Academy of Sciences, 184209 Apatity, Russia
[3] Skobeltsyn Institute of Nuclear Physics, Lomonosov Moscow State University, 119991 Moscow, Russia; dmitry.spasskiy@ut.ee
[4] Institute of Physics, University of Tartu, 50411 Tartu, Estonia
[5] Kola Science Centre, Geological Institute, Russian Academy of Sciences, 184209 Apatity, Russia
* Correspondence: aks.crys@gmail.com; Tel.: +7-8155575350

Abstract: A series of novel phosphates with the general formulas $Ca_9Gd_{0.9-x}Tm_{0.1}Sm_x(PO_4)_7$ and $Ca_9Gd_{0.9-y}Tm_ySm_{0.1}(PO_4)_7$ were synthesized by solid-state method. As-obtained phosphates were characterized by powder X-ray diffraction and second harmonic generation analyses, dielectric measurements, luminescence spectroscopy. All samples were single phase and characterized by the whitlockite-type structure with space group *R3c*. An influence of admixture concentration of REE^{3+} ions in the initial host on dielectric properties was studied in details. Synthesized phosphates are characterized by intensive luminescence. The emission in the orange region of the visible spectrum is observed for $Ca_9Gd_{0.9}Sm_{0.1}(PO_4)_7$ with a maximum intensity band at 602 nm. The line in blue region at 455 nm, which corresponds to $^1D_2 \rightarrow {}^3F_4$ Tm^{3+} transition, is registered for $Ca_9Gd_{0.9}Tm_{0.1}(PO_4)_7$. Emission in the white region of CIE coordinates was registered for Tm-Sm co-doped compounds.

Keywords: phosphates; luminescence spectroscopy; whitlockite-type compounds; energy transfer; cation distribution; thulium; samarium

Citation: Nikiforov, I.V.; Deyneko, D.V.; Spassky, D.A.; Lazoryak, B.I.; Aksenov, S.M. Whitlockite-Type Structure as a Matrix for Optical Materials: Synthesis and Characterization of Novel TM-SM Co-Doped Phosphate $Ca_9Gd(PO_4)_7$, a Single-Phase White Light Phosphors. *Minerals* **2022**, *12*, 76. https://doi.org/10.3390/min12010076

Academic Editor: Oleg I. Siidra

Received: 19 December 2021
Accepted: 6 January 2022
Published: 9 January 2022

1. Introduction

Inorganic oxysalts with the whitlockite-type structure [in particular, beta-tricalcium phosphate, β-$Ca_3(PO_4)_2$] attract interest due to different physical properties [1]. In the crystal structure of pure β-$Ca_3(PO_4)_2$ (space group *R3c*, Z = 21) Ca^{2+} ions occupy five non-equivalent *M*1–*M*5 sites [2,3]. The different types of Ca^{2+} substitutions by mono-, di- or trivalent cations make a significant influence on the physical properties (especially optical) [4,5] due to the local distortion of coordination environment of the central cations. Moreover, the variable occupancy of the M4 site (it can be either fully vacant or partially occupied up to half occupancy) makes it possible to change the symmetry of the crystal structure with the breaking of the symmetry center, which is important for the non-linear optical properties. The impact of cationic and anionic substitutions on luminescence properties has been studied previously in details [4,6]. It was shown that homo- and heterovalent substitutions occur without the change of β-$Ca_3(PO_4)_2$-type structure. However, in some compounds with β-$Ca_3(PO_4)_2$-type structure which contain cations of different oxidation states, the co-doping of admixture quantity ions is necessary to charge balance of the structure. Such doping may change physical properties and crystal structure [7].

During the last years, a number of studies were focused on heterovalent substitutions with the doping of the initial host by rare-earth elements (REE). REE ions are characterized

by emission in the visible region, arising due to 4*f*–4*f* or 5*d*–4*f* electron transitions. The main goal of such modifications is the crystal chemical design of novel inorganic phosphors for LED applications. The materials developed using the initial β-$Ca_3(PO_4)_2$ host doped with Tm^{3+} ions can be considered as potential blue phosphors excited by UV radiation [8,9], while the Sm^{3+}-doped phosphates show orange-red emission [10]. Moreover, the luminescent properties can be significantly improved by co-doping with other REE, such as Gd^{3+} [11] due to the energy transfer processes. Previously it was shown that co-doping by Gd^{3+} ions results in energy pump processes [11], high quantum yield [6], color tuning [12], and improving luminescence characteristics [6].

Among vanadates with the β-$Ca_3(PO_4)_2$-type structure, $Ca_9Gd(VO_4)_7$ is a good candidate as a host [13], and the influence of the co-doping by a Tm^{3+}–Sm^{3+} pair has been recently reported [14]. However, a similar study for the phosphate analog has not been published so far, and the role of Tm^{3+}–Sm^{3+} co-doping admixture on the crystal structure and phase transitions of $Ca_9Gd(PO_4)_7$ remains unknown. Despite the isostructurality of $Ca_3(PO_4)_2$ and $Ca_3(VO_4)_2$ phosphates are characterized by better chemical and thermal stability and environmental friendliness compared to vanadates. So, phosphates are more promising compounds for phosphors than other host-matrix, as vanadate [15].

The current study represents a complex analysis of phosphates with the formulas $Ca_9Gd_{0.9-x}Tm_{0.1}Sm_x(PO_4)_7$ and $Ca_9Gd_{0.9-y}Tm_ySm_{0.1}(PO_4)_7$ based on the means X-ray powder diffraction, the second harmonic generation as well as dielectric and luminescence spectroscopy.

2. Materials and Methods

Series of phosphates $Ca_9Gd_{0.9-x}Tm_{0.1}Sm_x(PO_4)_7$ ($Gd_{0.9-x}Tm_{0.1}Sm_x$, x = 0; 0.1; 0.2; 0.3) and $Ca_9Gd_{0.9-y}Tm_ySm_{0.1}(PO_4)_7$ ($Gd_{0.9-y}Tm_ySm_{0.1}$, y = 0; 0.1; 0.2; 0.3) were synthesized by a solid-state method in air from stoichiometric mixtures of $CaHPO_4{\cdot}2H_2O$ (99.9%), $CaCO_3$ (99.9%), REE_2O_3 (REE–Gd^{3+}, Tm^{3+}, Sm^{3+}) (99.99%) at 1150 °C for 100 h with several intermediate grindings. The precursors were controlled by the powder X-ray diffraction (PXRD) patterns, and no impurities were detected.

The PXRD patterns were collected on a Thermo ARL X'TRA powder diffractometer (Bragg–Brentano geometry, Scintillator detector, CuKα radiation, λ = 1.5418 Å, Thermo Fisher Scientific, Waltham MA, USA). The PXRD data were collected at room temperature in the 2θ range between 5° and 65° with a step interval of 0.02°. Crystallographic Search-Match and Jana2006 [16] programs were used to determine the unit cell parameters.

Photoluminescence emission (PL) and excitation (PLE) spectra were recorded using laboratory set-up based on a LOT-Oriel MS-257 spectrograph (L.O.T.-Oriel, Irvine, CA, USA) with a 75 kW xenon light source (pulse length τ = 2 μs, pulse frequency ν = 80 Hz, wavelength resolution 0.5 nm; photomultiplier tube (PMT) Hamamatsu R928). All measurements were performed at room temperature.

Dielectric permittivity ε and dielectric loss tangent tan δ in the air were measured by a double-contact method in the frequency range of 1–106 Hz at 300–1270 K (heating rate of 10 K/min), with the assistance of a Solartron 7081 precision voltmeter and a Solartron 1260 frequency response analyzer (Karpov Institute, Moscow, Russia). Ceramic pellets (1.5 mm-thick and 5–6 mm in diameter) were prepared by pressing and sintering at 1473 K for 12 h. Pt paste was applied to the flat surfaces of the pellets, and then, they were heated at 1023 K for 4 h to produce platinum electrodes.

The second harmonic generation (SHG) signal was measured with a *Q*-switched YAG: Nd laser at λ_ω =1064 nm in the reflection mode (Karpov Institute, Moscow, Russia) [17].

Scanning electron microscopy (SEM) (Tescan Analytics, Fuveau, France) observations were performed using a Tescan VEGA3 scanning electron microscope. SEM images were acquired using a secondary electron (SE) imaging and backscattered electron (BSE) imaging technique.

3. Results and Discussion

PXRD patterns of $Gd_{0.9-x}Tm_{0.1}Sm_x$ and $Gd_{0.9-y}Tm_ySm_{0.1}$ are shown in Figure 1. The number and positions of peaks correspond to $Ca_9Dy(PO_4)_7$ (PDF Card No 49-1086) for all as-synthesized solid solutions. Thus, the samples were single-phase and characterized by the whitlockite-type structure with polar space group (SG) *R3c* (depending on the structural feature of compounds with β-$Ca_3(PO_4)_2$-type structure may also crystallize in non-polar SG $R\bar{3}c$ [18]). PXRD patterns for both SGs are almost identical, and it is rather difficult to identify them based on the powder diffraction data only [19]. However, the noncentrosymmetric structure (described by the polar SG *R3c*) can be confirmed by SHG measurements. The presence of a weak SHG signal response (≈1–1.5 by quartz standard) for $Gd_{0.9-x}Tm_{0.1}Sm_x$ and $Gd_{0.9-y}Tm_ySm_{0.1}$ confirms that these samples are characterized by polar SG *R3c* (in case of the absence of SHG response the SG should be $R\bar{3}c$ [2]).

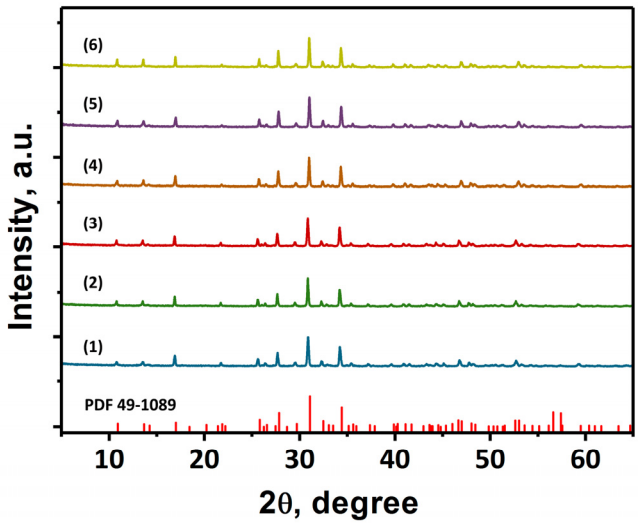

Figure 1. PXRD patterns for $Ca_9Gd_{0.9-x}Tm_{0.1}Sm_x(PO_4)_7$ (x = 0 (1); 0.2 (2); 0.3 (3)) and $Ca_9Gd_{0.9-y}Tm_ySm_{0.1}(PO_4)_7$ (y = 0 (4); 0.1 (5); 0.2 (6)) with Bragg reflections for $Ca_9Dy(PO_4)_7$ (PDF Card No 49-1086).

The calculated values of the unit cell volumes for $Gd_{0.9-x}Tm_{0.1}Sm_x$ and $Gd_{0.9-y}Tm_ySm_{0.1}$ are given in Figure 2. In comparison with pure $Ca_9Gd(PO_4)_7$ [20] the linear decrease of the unit cell volume with Tm^{3+} doping is observed for $Gd_{0.9-y}Tm_ySm_{0.1}$, while the increase of the unit cell volumes corresponds to Sm^{3+} doping of $Gd_{0.9-x}Tm_{0.1}Sm_x$. Such changes of the unit cell volumes can be explained by the substitution of Gd^{3+} ion (r_{VI} = 0.94 Å) by Tm^{3+} (r_{VI} = 0.88 Å) and Sm^{3+} (r_{VI} = 0.96 Å) with smaller and bigger ionic radius, respectively [21].

The relative ionic radius difference (D_r) characterizes an effective substitution in the crystal structure of the initial host. The D_r must be less than 30%. The value of relative ionic radius difference can be calculated by the following equation [3]:

$$D_r = \left| \frac{r_s - r_d}{r_s} \right| \times 100\%,$$

where r_s and r_d are ionic radii for substituted and dopant ion, respectively, with the same coordination number (CN). The obtained D_r values are given in Table 1 and do not exceed 30%. Thus, Tm^{3+} and Sm^{3+} can substitute Gd^{3+} and Ca^{2+} in the initial crystal structure. These data are in good agreement with the occupations of the crystallographic sites. In particular, the octahedral M5 site is occupied by Tm^{3+} jointly with Ca^{2+}, and the largest M1-M3 sites are statistically occupied by Gd^{3+}, Tm^{3+}, Sm^{3+}, and Ca^{2+} [20]. The cationic distribution in $Gd_{0.9-x}Tm_{0.1}Sm_x$ and $Gd_{0.9-y}Tm_ySm_{0.1}$ is based on D_r calculations. Despite the fact that the D_r value of Ca^{2+}/Sm^{3+} in the octahedral M5 site is less due to larger

similarity of the ionic radii, Tm^{3+} ions are preferably occupied it. The reason is the smaller difference in pair Ca^{2+}/Sm^{3+} (D_r = 3.7) in comparison with Ca^{2+}/Tm^{3+} (D_r = 13.1) in larger eight-coordinates sites M1-M3. So, the smallest size of Tm^{3+} ion is the argument to prefer occupation among other REE ions Gd^{3+} and Sm^{3+} in the synthesized compounds.

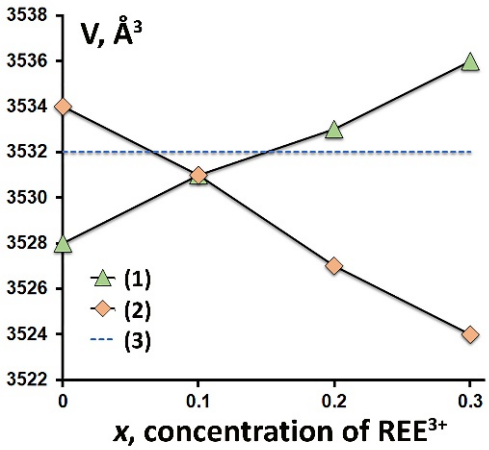

Figure 2. Dependence of the unit cell volumes of $Ca_9Gd_{0.9-x}Tm_{0.1}Sm_x(PO_4)_7$ (1) and $Ca_9Gd_{0.9-y}Tm_ySm_{0.1}(PO_4)_7$ (2) on the concentration of REE, and the unit cell volume of pure $Ca_9Gd(PO_4)_7$ (3).

Table 1. The ionic radii difference D_r between substituted and dopant ions.

Dopantion	Radius, Å/CN	D_r, %			
		Gd^{3+}		Ca^{2+}	
		1.05 Å/8	**0.94 Å/6**	**1.12 Å/8**	**1.00 Å/6**
Tm^{3+}	0.88/6	–	6.8	–	13.6
	0.99/8	6.1	–	13.1	–
Sm^{3+}	0.96/6	–	1.1	–	5.3
	1.08/8	2.7	–	3.7	–

Figure 3 shows the SEM image for $Gd_{0.8}Tm_{0.1}Sm_{0.1}$. Observed phosphate, as well as all as-prepared samples, is characterized by narrow size distribution in the interval from 10 to 100 μm with a large number of large particles.

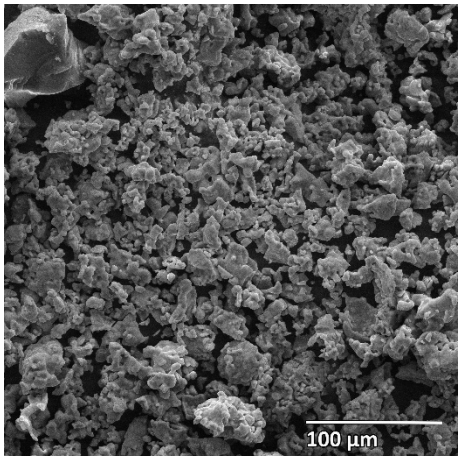

Figure 3. The SEM image for $Ca_9Gd_{0.8}Tm_{0.1}Sm_{0.1}(PO_4)_7$.

The temperature dependences of dielectric permittivity (ε) and dielectric loss tangent (tan δ) for pure $Ca_9Gd(PO_4)_7$ are shown in Figure 4. The maxima at the ε(T) curves may indicate the phase transition (PT). The presence of anomalies in the tan δ curves demonstrates the type of PT, which can be determined as ferroelectric type. So, the PT is observed with SG $R3c \rightarrow R\bar{3}c$ changing for $Ca_9Gd(PO_4)_7$. The temperature of PT, determined by maxima and minima in ε(T) and tan δ(T) curves, respectively, takes value of 850 K. The similar behaviors have been also found for $Gd_{0.9-x}Tm_{0.1}Sm_x$and $Gd_{0.9-y}Tm_ySm_{0.1}$ samples. The temperatures of PT vary between 850 K to 865 K for as-synthesized phosphates. The obtained data might be considered as equal due to instrumental error (20 K). The significant changes in PT were not detected with doping by admixture concentration of Tm^{3+} and Sm^{3+}.

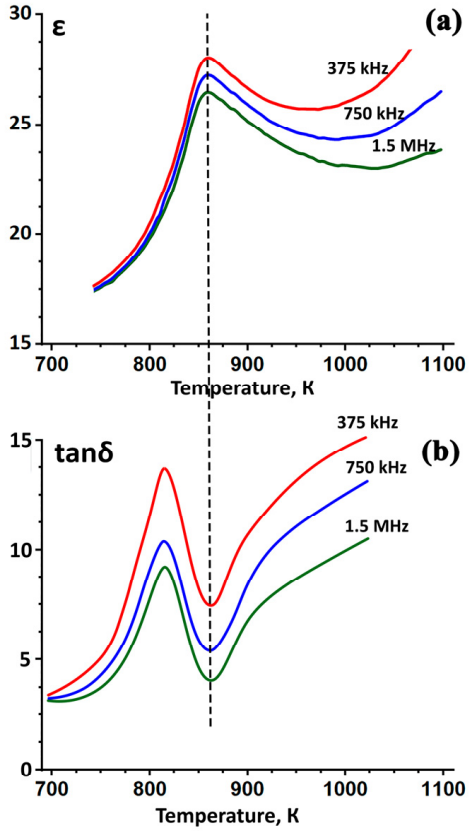

Figure 4. Temperature dependence of the dielectric permittivity ε (**a**) and dielectric loss tangent tan δ (**b**) for $Ca_9Gd(PO_4)_7$.

The PLE spectrum of $Gd_{0.9}Sm_{0.1}$, recorded at λ_{em} = 602 nm, is given in Figure 5a. The series of sharp lines in the region of 300–500 nm correspond to *f–f* transitions within Sm^{3+} ions. The bands at 346, 363, 375, 404, 416, 439, and 475 nm correspond to Sm^{3+} transitions from the $^6H_{5/2}$ ground level to the excited levels $^4H_{13/2}$, $^4D_{3/2}$, $^6P_{7/2}$, $^4F_{7/2}$, $^6P_{5/2}$, $^4G_{9/2}$, and $^4I_{11/2}$, respectively [22,23]. The most intensive $^6H_{5/2} \rightarrow {}^4F_{7/2}$ transition is located at 404 nm.

At PL spectrum of $Gd_{0.9}Sm_{0.1}$, registered at λ_{ex} = 404 nm, a standard set of emission lines, which arise due to transitions within Sm^{3+} ions is observed (Figure 5b). The emission bands in the visible orange-red spectral region peaking at 563, 602, 644 and 704 nm correspond to $^4G_{5/2} \rightarrow {}^4H_{J/2}$ (J = 5, 7, 9, 11) transitions within Sm^{3+} ions [22,23]. The dominant line was found at 602 nm ($^4G_{5/2} \rightarrow {}^4H_{7/2}$). The 4f-4f transitions of REE^{3+} are almost insensitive to the changing of the crystal field strength, and the profile and relative intensities of the Sm^{3+} related emission bands were similar for all studied series. The main

difference between the samples was in the integral emission intensity, which is ascribed to the energy transfer processes.

The PLE spectrum of $Gd_{0.9}Tm_{0.1}$, monitored at λ_{em} = 477 nm, is presented in Figure 6a. The spectrum demonstrates an expressed band at 356 nm, corresponding to $^3H_6 \rightarrow {}^1D_2$ transition within Tm^{3+}. The onset observed below 300 nm might be attributed to the defect-related absorption. The characteristic emission line, corresponding to 4*f*–4*f* transition within Tm^{3+} is observed at PL spectrum (Figure 6b). This band is located at 455 nm and is due to $^1D_2 \rightarrow {}^3F_4$ transition [14,24,25].

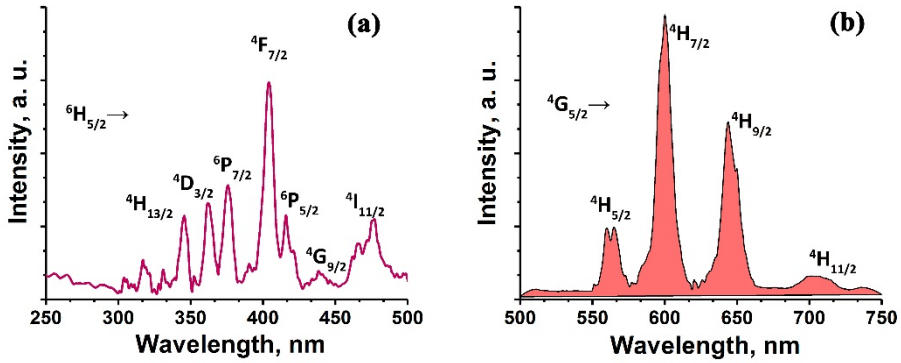

Figure 5. (**a**) PLE (λ_{em} = 602 nm) and (**b**) PL (λ_{ex} = 404 nm) spectra for $Ca_9Gd_{0.9}Sm_{0.1}(PO_4)_7$.

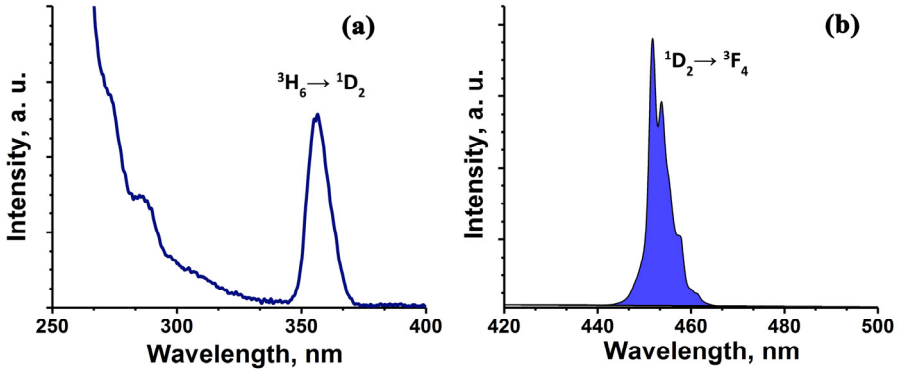

Figure 6. (**a**) PLE (λ_{em} = 477 nm) and (**b**) PL (λ_{ex} = 356 nm) spectra for $Ca_9Gd_{0.9}Tm_{0.1}(PO_4)_7$.

The emission bands of Tm^{3+} and Sm^{3+} ions, are registered in PL spectrum of $Gd_{0.8}Tm_{0.1}Sm_{0.1}$ at λ_{ex} = 356 nm, which corresponds to intracenter excitation of Tm^{3+} ions (Figure 7). Thus, energy transfer from Tm^{3+} to Sm^{3+} occurs. In contrast, energy transfer from Sm^{3+} to Tm^{3+} is not registered, which is confirmed by the absence of Tm^{3+} emission lines under excitation at λ_{ex} = 404 nm (Sm^{3+} intracenter excitation).

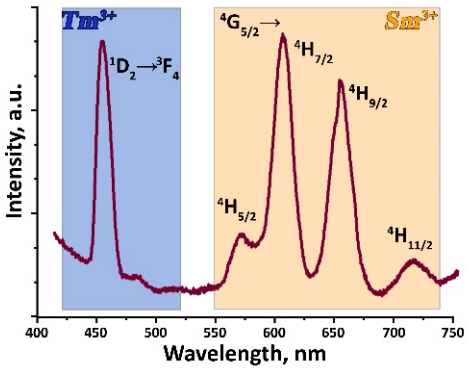

Figure 7. PL spectrum of $Ca_9Gd_{0.8}Tm_{0.1}Sm_{0.1}(PO_4)_7$, λ_{ex} = 356 nm.

The data on the intensity dependence of Tm^{3+} and Sm^{3+} emission on the REE concentrations are presented in Figure 8. The intensity of Sm^{3+} emission for $Gd_{0.9-x}Tm_{0.1}Sm_x$ samples increases with x. At the same time, the intensity of Tm^{3+} emission decreases while its concentration doesn't change (Figure 8a). Such behavior indicates the possibility of energy transfer from Tm^{3+} to Sm^{3+} under at 356 nm, which correspond to Tm^{3+} intraceneter excitation. It is worth noting that the intensity of Sm^{3+} emission is nonzero (Figure 8b) at λ_{ex} =356 nm even for $Gd_{0.9}Sm_{0.1,}$ (i.e. without Tm^{3+} ions in the sample) that is due to the presence of a Sm^{3+} excitation band at 356 nm. The increase of the Sm^{3+} emission is observed with the incorporation of Tm^{3+} into studied phosphates for the sample $Gd_{0.8}Tm_{0.1}Sm_{0.1}$. The observed intensity increase also indicates the existence of an energy transfer process from Tm^{3+} to Sm^{3+}. However, the intensity of Sm^{3+} emission decreases with a further increase of the Tm^{3+} concentration in the host.

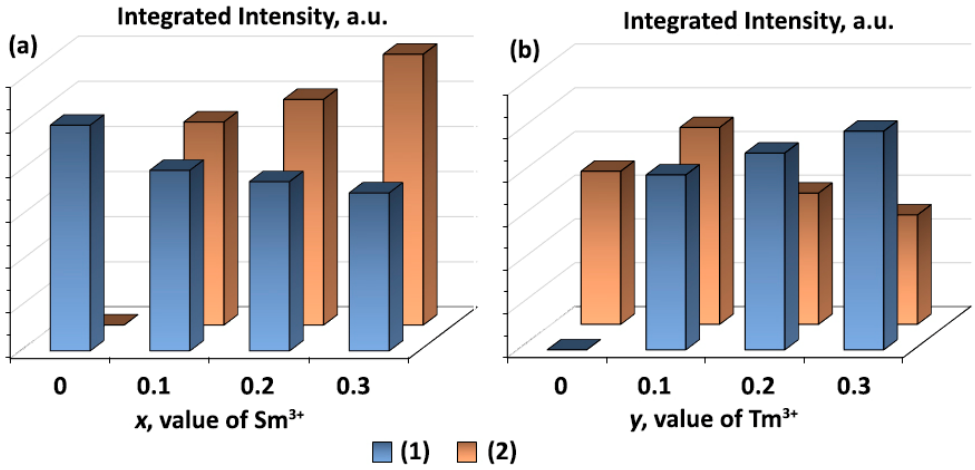

Figure 8. Integrated intensity of Tm^{3+} (1) and Sm^{3+} (2) emissions for $Ca_9Gd_{0.9-x}Tm_{0.1}Sm_x(PO_4)_7$ (**a**) and $Ca_9Gd_{0.9-y}Tm_ySm_{0.1}(PO_4)_7$ (**b**) at λ_{ex} = 356 nm.

CIE coordinates (x, y, z) show the color of emission for phosphors, according to international standards. They were calculated using the following equation [26]:

$$x = \frac{X}{X+Y+Z}; y = \frac{Y}{X+Y+Z}; z = \frac{Z}{X+Y+Z};$$

where

$$X = \int_{\lambda_{inf}}^{\lambda_{sup}} S(\lambda)\overline{x}(\lambda)d(\lambda);\ Y = \int_{\lambda_{inf}}^{\lambda_{sup}} S(\lambda)\overline{y}(\lambda)d(\lambda);\ Z = \int_{\lambda_{inf}}^{\lambda_{sup}} S(\lambda)\overline{z}(\lambda)d(\lambda)$$

where $S(\lambda)$ is the intensity at wavelength λ; $\overline{x}$, $\overline{y}$, $\overline{z}$ are color 1931CIE coordinates (CIE coordinates) at wavelength λ; d is integration stp.

The calculated color coordinates (x, y) are presented in Figure 9. The CIE value for $Gd_{0.9}Tm_{0.1}$ is (0.17; 0.07) and corresponds to the blue region of the color space, while (0.53; 0.37) for $Gd_{0.9}Sm_{0.1}$ — to the orange region. The adjusting of Sm^{3+} concentration shifts the color coordinates from a blue region, through a near white one, to an orange one for $Gd_{0.9-x}Tm_{0.1}Sm_x$. This behavior can be explained by the redistribution of Sm^{3+} and Tm^{3+} emission bands intensity under λ_{ex} = 356 nm.

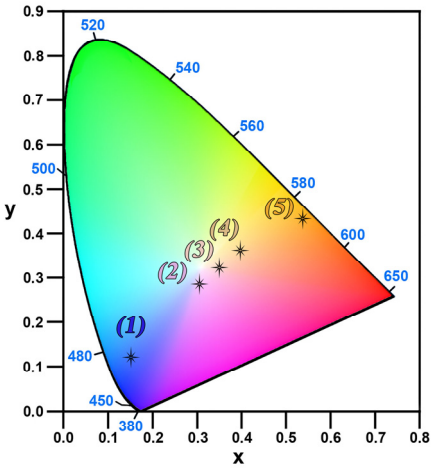

Figure 9. Color coordinates for $Ca_9Gd_{0.9-x}Tm_{0.1}Sm_x(PO_4)_7$ $x = 0$ (1), $x = 0.1$ (2), $x = 0.2$ (3), $x = 0.3$ (4) and $Ca_9Gd_{0.9}Sm_{0.1}(PO_4)_7$ (5).

4. Conclusions

Novel $Ca_9Gd_{0.9-x}Tm_{0.1}Sm_x(PO_4)_7$ ($x = 0$; 0.1; 0.2; 0.3) and $Ca_9Gd_{0.9-y}Tm_ySm_{0.1}(PO_4)_7$ ($y = 0$; 0.1; 0.2; 0.3) phosphates with β-$Ca_3(PO_4)_2$-type structure were synthesized by a solid-state technique. It was found that the admixture concentration of REE ions in the initial host does not influence on the formation of the whitlockite-type structure and dielectric properties. The temperature of phase transitions is 850–865 K for as-prepared samples. The REE emitting-ions can be exctied by ultraviolet radiation being in admixture quantity in the whitlockite-type host. The typical emissions in the orange (the most intensive band at 602 nm) and the blue (the most intensive band at 455 nm) spectral regions were observed for $Ca_9Gd_{0.9}Sm_{0.1}(PO_4)_7$ and $Ca_9Gd_{0.9}Tm_{0.1}(PO_4)_7$, respectively. The energy transfer from Tm^{3+} to Sm^{3+} was detected for $Ca_9Gd_{0.9-y}Tm_ySm_{0.1}(PO_4)_7$ solid solution. It is shown that the resulting emission in the near-white area of CIE coordinates can be achieved by tuning of Sm^{3+} concentration in the $Ca_9Gd_{0.9-x}Tm_{0.1}Sm_x(PO_4)_7$ solid solutions.

Author Contributions: Conceptualization, I.V.N., D.A.S. and D.V.D.; methodology, D.V.D. and S.M.A.; synthesis, I.V.N.; formal analysis, I.V.N., D.V.D. and D.A.S.; writing—original draft preparation, I.V.N. and D.V.D.; writing—review and editing, B.I.L., D.A.S. and S.M.A.; supervision, D.V.D. All authors have read and agreed to the published version of the manuscript.

Funding: This research was supported by the Russian Science Foundation (Grant 19-77-10013). D.A.S. is grateful for financial support of the Estonian Research Council, project PUT PRG111. This research was performed according to the Development Program of the Interdisciplinary Scientific and Educational School of Lomonosov Moscow State University's "The future of the planet and global environmental change" and the state assignment of the Chemistry Department of Moscow State University (Agreement No. AAAA-A21-121011590086-0).

Conflicts of Interest: The authors declare no conflict of interest.

References

1. Teterskii, A.V.; Stefanovich, S.Y.; Lazoryak, B.I.; Rusakov, D.A. Whitlockite solid solutions $Ca_{9-x}M_xR(PO_4)_7$ (x = 1, 1.5; M = Mg, Zn, Cd; R = Ln, Y) with antiferroelectric properties. *Russ. J. Inorg. Chem.* **2007**, *52*, 308–314. [CrossRef]
2. Deyneko, D.V.; Aksenov, S.M.; Nikiforov, I.V.; Stefanovich, S.Y.; Lazoryak, B.I. Symmetry inhomogeneity of $_{Ca9-x}Zn_xEu(PO_4)_7$ phosphor determined by second-harmonic generation and dielectric and photoluminescence spectroscopy. *Cryst. Growth Des.* **2020**, *20*, 6461–6468. [CrossRef]
3. Nikiforov, I.V.; Deyneko, D.V.; Duskaev, I.F.; Lazoryak, B.I. Green luminophors in the family of phosphates with whitlockite structure. *J. Struct. Chem.* **2021**, *62*, 1621–1630. [CrossRef]
4. Lazoryak, B.I.; Zhukovskaya, E.S.; Baryshnikova, O.V.; Belik, A.A.; Leonidova, O.N.; Deyneko, D.V.; Savon, A.E.; Dorbakov, N.G.; Morozov, V.A. Luminescence, structure and antiferroelectric-type phase transition in $Ca_8ZnEu(PO_4)_7$. *Mater. Res. Bull.* **2018**, *104*, 20–26. [CrossRef]

5. Deyneko, D.V.; Morozov, V.A.; Hadermann, J.; Savon, A.E.; Spassky, D.A.; Stefanovich, S.Y.; Belik, A.A.; Lazoryak, B.I. A novel red $Ca_{8.5}Pb_{0.5}Eu(PO_4)_7$ phosphor for light emitting diodes application. *J. Alloy. Compd.* **2015**, *647*, 965–972. [CrossRef]
6. Deyneko, D.V.; Nikiforov, I.; Lazoryak, B.I.; Spassky, D.A.; Leonidov, I.I.; Stefanovich, S.Y.; Petrova, D.A.; Aksenov, S.M.; Burns, P.C. $Ca_8MgSm_{1-x}(PO_4)_7$: xEu^{3+}, promising red phosphors for WLED application. *J. Alloy. Compd.* **2019**, *776*, 897–903. [CrossRef]
7. Deyneko, D.V.; Spassky, D.A.; Morozov, V.A.; Aksenov, S.M.; Kubrin, S.P.; Molokeev, M.S.; Lazoryak, B.I. Role of the Eu^{3+} distribution on the properties of β-$Ca_3(PO_4)_2$ phosphors: Structural, luminescent, and 151Eu Mössbauer spectroscopy study of $Ca_{9.5-1.5x}MgEu_x(PO_4)_7$. *Inorg. Chem.* **2021**, *60*, 3961–3971. [CrossRef]
8. Xie, F.; Xu, D.; Wu, Z.; Molokeev, M.S.; Milićević, B.; Li, H.; Shi, J. Improving thermal stability of novel single-component white-light emitting phosphor $Ca_8MgLu(PO_4)_7$:Tm^{3+}, Dy^{3+} by back-energy-transfer. *J. Lumin.* **2020**, *227*, 117516. [CrossRef]
9. Zhang, J.; Wang, Y.; Guo, L.; Zhang, F.; Wen, Y.; Liu, B.; Huang, Y. Vacuum ultraviolet and near-infrared excited luminescence properties of $Ca_3(PO_4)_2$:RE^{3+}, Na^+ (RE = Tb, Yb, Er, Tm, and Ho). *J. Solid State Chem.* **2011**, *184*, 2178–2183. [CrossRef]
10. Zhang, Z.-W.; Wu, Y.-N.; Shen, X.-H.; Ren, Y.-J.; Zhang, W.-G.; Wang, D.-J. Enhanced novel orange red emission in $Ca_3(PO_4)_2$:Sm^{3+} by charge compensation. *Opt. Laser Technol.* **2014**, *62*, 63–68. [CrossRef]
11. Xie, M.; Liang, H.; Huang, Y.; Gao, Z.; Tao, Y. Host absorption sensitizing and energy transfer to Eu^{3+} by Gd^{3+} in $Ba_6Gd_{2-x}Na_2Eu_x(PO_4)_6F_2$. *J. Solid State Chem.* **2013**, *201*, 18–23. [CrossRef]
12. Guo, N.; Liang, Q.; Li, S.; Ouyang, R.; Lü, W. Triple energy transfer and color tuning in Tb^{3+} and Eu^{3+}-coactivated apatite-type gadolinium-containing phosphors. *Opt. Mater.* **2017**, *73*, 570–576. [CrossRef]
13. Paszkowicz, W.; Shekhovtsov, A.; Kosmyna, M.; Loiko, P.; Vilejshikova, E.; Minikayev, R.; Romanowski, P.; Wierzchowski, W.; Wieteska, K.; Paulmann, C.; et al. Structure and thermal expansion of $Ca_9Gd(VO_4)_7$: A combined powder-diffraction and dilatometric study of a Czochralski-grown crystal. *Nucl. Instrum. Methods Phys. Res. Sect. B Beam Interact. Mater. At.* **2017**, *411*, 100–111. [CrossRef]
14. Liu, X.; Li, L.; Noh, H.M.; Jeong, J.H.; Jang, K.; Shin, D.S. Chemical bond parameters, charge transfer band, tunable white light of Tm^{3+} and Sm^{3+} coactivated $Ca_9Gd(VO_4)_7$. *J. Alloy. Compd.* **2015**, *618*, 649–655. [CrossRef]
15. Zhang, Z.Z.; Zhang, F.; Li, G.Q.; Zhang, J.; Zhang, W.F. Red-emitting phosphor series: $Ca_9Y(PO_4)_{7(1-x)}(VO_4)_{7x}$: Eu^{3+} (x = 0−1) with improved luminescence thermal stability by anionic polyhedron substitution. *J. Mater. Sci. Mater. Electron.* **2019**, *30*, 8838–8846. [CrossRef]
16. Petříček, V.; Dušek, M.; Palatinus, L. Crystallographic computing system JANA2006: General features. *Z. Krist. Cryst. Mater.* **2014**, *229*, 345–352. [CrossRef]
17. Deyneko, D.V.; Nikiforov, I.V.; Spassky, D.A.; Berdonosov, P.S.; Dzhevakov, P.B.; Lazoryak, B.I. $Sr_8MSm_{1-x}Eu_x(PO_4)_7$ phosphors derived by different synthesis routes: Solid state, sol-gel and hydrothermal, the comparison of properties. *J. Alloy. Compd.* **2021**, *887*, 161340. [CrossRef]
18. Dikhtyar, Y.Y.; Deyneko, D.V.; Boldyrev, K.N.; Borovikova, E.Y.; Lipatiev, A.S.; Stefanovich, S.Y.; Lazoryak, B.I. Luminescent properties of Er^{3+} in centrosymmetric and acentric phosphates $Ca_8MEr(PO_4)_7$ (M = Ca, Mg, Zn) and $Ca_{9-x}Zn_xLa(PO_4)_7$:Er^{3+}. *Mater. Res. Bull.* **2021**, *138*, 111244. [CrossRef]
19. Deyneko, D.V.; Nikiforov, I.; Spassky, D.; Dikhtyar, Y.Y.; Aksenov, S.M.; Stefanovich, S.Y.; Lazoryak, B.I. Luminescence of Eu^{3+} as a probe for the determination of the local site symmetry in β-$Ca_3(PO_4)_2$-related structures. *CrystEngComm* **2019**, *21*, 5235–5242. [CrossRef]
20. Bessière, A.; Benhamou, R.A.; Wallez, G.; Lecointre, A.; Viana, B. Site occupancy and mechanisms of thermally stimulated luminescence in $Ca_9Ln(PO_4)_7$ (Ln=lanthanide). *Acta Mater.* **2012**, *60*, 6641–6649. [CrossRef]
21. Shannon, R. Revised effective ionic radii and systematic study of inter atomic distances in halides and chalcogenides. *Acta Crystallogr. Sect. A Found. Crystallogr.* **1976**, *32*, 751–767.
22. Zhang, Z.-J.; Yang, W. Luminescence characteristic of RE (RE = Pr, Sm, Eu, Tb, Dy) and energy levels of lanthanide ions in $Gd_5Si_3O_{12}N$. *Solid State Sci.* **2017**, *72*, 64–70. [CrossRef]
23. Zhang, J.; Wang, Y.; Wen, Y.; Zhang, F.; Liu, B. Luminescence properties of $Ca_{10}K(PO_4)_7$:RE^{3+} (RE=Ce, Tb, Dy, Tm and Sm) under vacuum ultraviolet excitation. *J. Alloy. Compd.* **2011**, *509*, 4649–4652. [CrossRef]
24. Gruber, J.B.; Conway, J.G. Electronic energy levels and crystal quantum states of Tm (IV). *J. Chem. Phys.* **1960**, *32*, 1178. [CrossRef]
25. Baklanova, Y.V.; Lipina, O.A.; Surat, L.L.; Chufarov, A.Y.; Tyutyunnik, A.P.; Zubkov, V.G. Luminescence Properties of $Sr_2La_{8-x}Tm_x(GeO_4)_6O_2$ Apatites (x = 0.1–1.0) in the Visible and Short-Wave IR Spectral Ranges. *Phys. Solid State* **2020**, *62*, 1407–1414. [CrossRef]
26. Ferhi, M.; Horchani-Naifer, K.; Férid, M. Spectroscopic properties of Eu^{3+}-doped $KLa(PO_3)_4$ and $LiLa(PO_3)_4$ powders. *Opt. Mater.* **2011**, *34*, 12–18. [CrossRef]